

SCATTERING OF LIGHT FROM HOLLOW AND SEMI-HOLLOW 3D SCATTERERS WITH ELLIPSOIDAL, CYLINDRICAL AND CARTESIAN SYMMETRIES

Xi Chen¹, Olga Korotkova¹

¹Department of Physics, University of Miami, Coral Gables, FL 33146, USA

Abstract

Scattering potentials of hollow particles with ellipsoid-, cylinder- and parallelepiped-like shapes and adjustable edge sharpness are introduced as a difference of two 3D multi-Gaussian functions with suitable parameters. The far-zone intensity distributions generated on weak scattering from such potentials are shown to depend on the scatterer's boundary thickness, edge softness as well as on its size relative to the wavelength. Possible extension to potentials formed by nested shells of the same or different types and potentials with semi-hollow center is outlined.

Keywords: scattering, particles.

Citation: Chen X, Korotkova O. Scattering of light from hollow and semi-hollow 3D scatterers with ellipsoidal, cylindrical and cartesian symmetries. *Computer Optics* 2016; 40(5): 635-641. DOI: 10.18287/2412-6179-2016-40-5-635-641.

Acknowledgement: O. Korotkova's research is funded by Air Force Office of Scientific Research (AFOSR) (FA9550-12-1-0449).

Introduction

The classic Mie theory of plane wave scattering from uniform solid spheres [1] has led to closed form solutions for the angular distribution of the scattered energy depending on the wavelength of light as well as the size and the refractive index of the particle. The Mie solution predicted the redistribution of the incident uniform energy field into the fringe-like far-zone pattern with several well-pronounced dark concentric circles centered about the incident wave's direction and appearing when the scatterer's size is somewhat greater than the light's wavelength. The important extensions of the Mie theory were later reported for scattering from soft spheres, hollow spheres, collections of spheres, cylinders [10]. Light scattering from particles with various physical and statistical properties remains the topic of acute scientific interest [2]–[9].

In recent publications [11, 12] the attempt was made to predict the outcome of plane wave scattering from particles with different 3D shapes and adjustable edge sharpness covering the broad class of potentials from soft (Gaussian) to hard (step-like). This was achieved with the help of the 3D multi-Gaussian distributions for the scattering potentials being weighed sums of positive and negative Gaussian function with well-chosen widths. It was shown that as the multi-Gaussian function approaches the step function limit, the solution in [11, 12] tends to the Mie solution exhibiting strong interference-like scattered intensity distribution.

The purpose of this paper is to explore the result of scattering from hollow 3D potentials with ellipse, cylinder and parallelepiped-like shapes with adjustable inner and outer edge sharpness. The dependence of the scattered angular intensity distribution on the particle size, shape, edge sharpness and the shell's thickness is to be examined in detail. Our results are based on the first Born approximation [13] and can accurately predict the outcomes only in the situations when the refractive index within the scatterer is sufficiently close to unity.

The practical importance of this study is in modeling of a number of airborne, underwater and bio-tissue based particles that have slightly different refraction index from its

surrounding medium and either fully or partially hollow. Moreover, the convenience of fine tuning of the model to the particle's outer and inner edge sharpness profiles allows to treat practically all the optically soft particles with three basic types of 3D symmetry. In cases when the particulate collections of deterministic or random nature are to be accounted for the simple superposition of potentials with spatially different centers can be employed.

1. Weak scattering theory

In the scattering theory a particle occupying domain D and having the refractive index distribution $n(\mathbf{r}, \omega)$, where $\mathbf{r} = (x, y, z)$ is the location in space and ω is the angular frequency, may be characterized by its scattering potential [13]

$$F(\mathbf{r}, \omega) = \begin{cases} (k^2 / 4\pi) [n^2(\mathbf{r}, \omega) - 1], & \mathbf{r} \in D, \\ 0, & \text{otherwise,} \end{cases} \quad (1)$$

where $k = \omega/c$ is the wave number, c being the speed of light in vacuum.

If the monochromatic plane wave

$$U^{(i)}(\mathbf{r}, \omega) = a^{(i)}(\omega) \exp[i\mathbf{k}\mathbf{s}_0 \cdot \mathbf{r}] \quad (2)$$

with amplitude $a^{(i)}(\omega)$ is incident from direction \mathbf{s}_0 ($|\mathbf{s}_0| = 1$) onto a deterministic stationary particle with potential (1) then the far-zone intensity of the weakly-scattered field, measured along direction $\mathbf{r} = r\mathbf{s}$ ($|\mathbf{s}| = 1, |\mathbf{r}| = 1$), can be expressed as [13]

$$S^{(s)}(r\mathbf{s}, \omega) = \frac{1}{r^2} S^{(i)}(\omega) \left| \tilde{F}[k(\mathbf{s} - \mathbf{s}_0), \omega] \right|^2, \quad (3)$$

where $S^{(i)}(\omega)$ is the spectrum of the incident light, \tilde{F} is the three-dimensional spatial Fourier transform

$$\tilde{F}(\mathbf{K}) = \int_D F(\mathbf{r}'; \omega) \exp[-i\mathbf{K} \cdot \mathbf{r}'] d^3r', \quad (4)$$

and $\mathbf{K} = k(\mathbf{s} - \mathbf{s}_0)$ is the momentum transfer vector.

2. Spherically symmetric potentials

We begin the discussion from the simplest situation when the hollow semi-hard edge potential is spherically symmetric:

$$F_{HS}(\mathbf{r}; \omega) = \frac{k^2}{4\pi C_l} \sum_{l=1}^L (-1)^{l-1} \binom{L}{l} \times [h_o \exp\left[-l \frac{x^2 + y^2 + z^2}{2\sigma_o^2}\right] - h_i \exp\left[-l \frac{x^2 + y^2 + z^2}{2\sigma_i^2}\right]] \quad (5)$$

where h_o is the maximum value of the potential, h_i is such that $h_o > h_i$, $h_o - h_i$ is the minimum value of the potential (at the particle's center), σ_o is the radius of the outer edge, $\sigma_i > \sigma_o$, $\sigma_o - \sigma_i$ defines the thickness (fill factor) of the shell and a normalization factor is

$$C_l = \sum_{l=1}^L (-1)^{l-1} \binom{L}{l}, \quad (6)$$

where $\binom{L}{l}$ are binomial coefficients.

We note that the series in Eq. (5) may be equivalently written as a single function. Indeed, if

$$f(u) = 1 - (1-u)^L, \quad (7)$$

where u is a scalar variable and L is a positive integer, one may represent $f(u)$ via finite series

$$f(u) = -\sum_{l=1}^L \binom{L}{l} (-u)^l. \quad (8)$$

In function u (in one dimension) is chosen as:

$$u(x) = \exp\left[-\frac{x^2}{2\sigma^2}\right]. \quad (9)$$

then $f(x) = \sum_{l=1}^L (-1)^{l-1} \binom{L}{l} \exp\left[-l \frac{x^2}{2\sigma_x^2}\right]. \quad (10)$

To obtain the angular distribution of the spectral intensity of a plane wave scattered by sphere-like semi-soft particles we substitute the model of the potentials (5) into Eq. (3), and find that

$$S_{HS}^{(s)}(\mathbf{r}\mathbf{s}; \omega) = \frac{S^{(i)k^2}(\omega)}{4\pi r^2} \left\{ h_o \frac{(2\pi)^{3/2} \sigma_o^3}{C_l} \sum_{l=1}^L \frac{(-1)^{l-1}}{l^{3/2}} \binom{L}{l} \times \exp\left[\frac{-k^2 \sigma_o^2}{2l} [(\mathbf{s}_x - \mathbf{s}_{0x})^2 + (\mathbf{s}_y - \mathbf{s}_{0y})^2 + (\mathbf{s}_z - \mathbf{s}_{0z})^2]\right] - h_i \frac{(2\pi)^{3/2} \sigma_i^3}{C_l} \sum_{l=1}^L \frac{(-1)^{l-1}}{l^{3/2}} \binom{L}{l} \times \exp\left[\frac{-k^2 \sigma_i^2}{2l} \times [(\mathbf{s}_x - \mathbf{s}_{0x})^2 + (\mathbf{s}_y - \mathbf{s}_{0y})^2 + (\mathbf{s}_z - \mathbf{s}_{0z})^2]\right] \right\} \quad (11)$$

The spectral intensity of a plane wave is always nonnegative, so the following condition must be satisfied.

$$h_o \sigma_o^3 - h_i \sigma_i^3 \geq 0 \quad (12)$$

And this is automatically satisfied because of the previous condition.

Figures 1–4 show spherically symmetric potentials F_{HS} for different values of the summation index L , size σ_o , shell's thickness and shell's fill factor and the corresponding scattered intensity distributions.

For all the numerical examples we assume that the plane wave with wavelength $\lambda = 632$ nm is incident on scatterers with centers at $x=0$, $y=0$, and $z=0$ and $h_o = 1$, along direction \mathbf{s}_0 with coordinates $s_{0x} = \sin\theta_0 \cos\phi_0$, $s_{0y} = \sin\theta_0 \sin\phi_0$, $s_{0z} = \cos\theta_0$, where θ_0 and ϕ_0 are the polar and azimuthal incident angles in the corresponding spherical system. The scattered field is then calculated for a direction specified by a unit vector \mathbf{s} with coordinates $s_x = \sin\theta \cos\phi$, $s_y = \sin\theta \sin\phi$, $s_z = \cos\theta$, where θ and ϕ are the polar and azimuthal scattered angles.

Figure 1 shows the hollow scattering potentials with spherical symmetry and different number of terms, L in the summation and the corresponding scattered far fields. As L , and hence, the edge sharpness, grow the number of fringes increase but saturate to eight for the whole angular range of forwarding directions.

Figure 2 illustrates the dependence of the scattered intensity on the effective radius of the spherical shell with $L = 40$, $h_i = 1$ (completely hollow in the center), but with different values of σ_o and σ_i (for all cases $m a_o / \sigma_i = 5$).

For shells with σ_o smaller than $1/k$ the intensity decreases monotonically with azimuthal angle θ ; for the shells with sizes comparable or greater than $1/k$ the interference patterns are formed, with increasing number of dark fringes for larger shells.

In Figure 3 the potentials of different thickness and the corresponding far-zone scattered intensity distributions are presented. As thickness increases, the hollow potential approaches solid potential, leading to smaller number of dark fringes occurring at large azimuthal angles.

Figure 4 illustrates the capability of the model to predict the scattered intensity in cases when the center of the particle is partially filled. For this the value of h_i is to be positive. On fixing $L = 40$, $\sigma_o = 10/k$ and $\sigma_i = 5/k$ and varying h_i from 0 to 1, we find that for completely hollow and for semi-hollow particles the number of dark fringes is smaller than for the corresponding solid particle.

In order to extend the analysis from spherically symmetric shells to other 3D shapes we can use the same idea as in Ref. [12] based on arranging the multi-Gaussian summations as: single 3D (ellipsoid), (2+1)D (cylinder) and (1+1+1)D (parallelepiped). Of course, for hollow and semi-hollow potentials instead of single summations the differences of the sums are to be implemented.

3. Hollow ellipsoids

A scattering potential of an ellipsoidal scatterer with adjustable size, thickness, edge softness and fill factor can be modeled by the distribution:

$$F_{HE}(\mathbf{r}; \omega) = \frac{k^2}{4\pi C_l} \sum_{l=1}^L (-1)^{l-1} \binom{L}{l} \times \left\{ h_o \exp\left[-l \left(\frac{x^2}{2\sigma_{x_o}^2} + \frac{y^2}{2\sigma_{y_o}^2} + \frac{z^2}{2\sigma_{z_o}^2}\right)\right] - h_i \exp\left[-l \left(\frac{x^2}{2\sigma_{x_i}^2} + \frac{y^2}{2\sigma_{y_i}^2} + \frac{z^2}{2\sigma_{z_i}^2}\right)\right] \right\}. \quad (13)$$

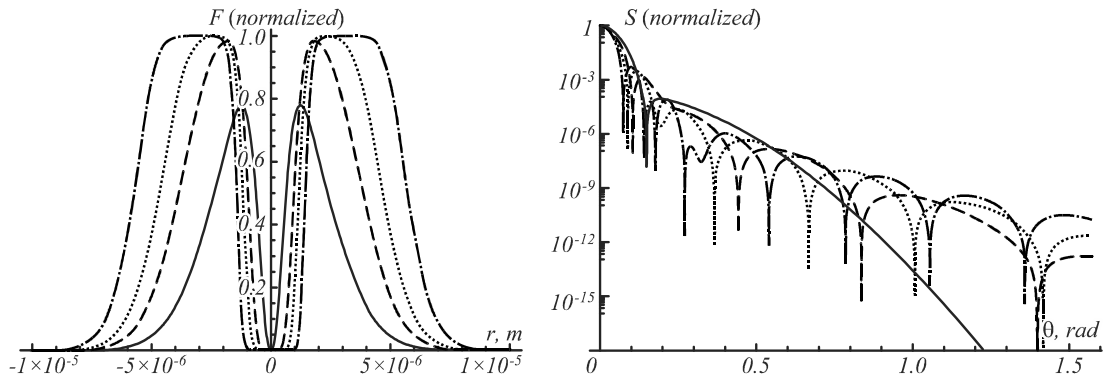


Fig. 1. The potential and the intensity of the scattered plane wave for $\sigma_o = 20/k$, $\sigma_i = 5/k$, $h_o = h_i = 1$, with $L = 1$ (solid curve), $L = 4$ (dashed curve), $L = 10$ (dotted curve) and $L = 40$ (dash-dotted curve)

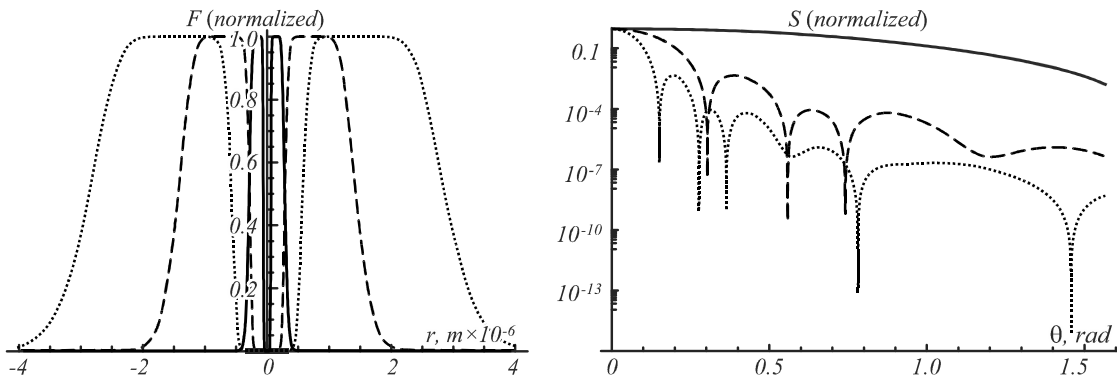


Fig. 2. The potential and the intensity of the scattered plane wave for $L = 40$ and different sizes: $\sigma_o = 1/k$, $\sigma_i = 0.2/k$ (solid curve); $\sigma_o = 5/k$ (dashed curve), $\sigma_i = 1/k$ (dash-dotted curve); and $\sigma_o = 10/k$, $\sigma_i = 2/k$ (dotted curve)

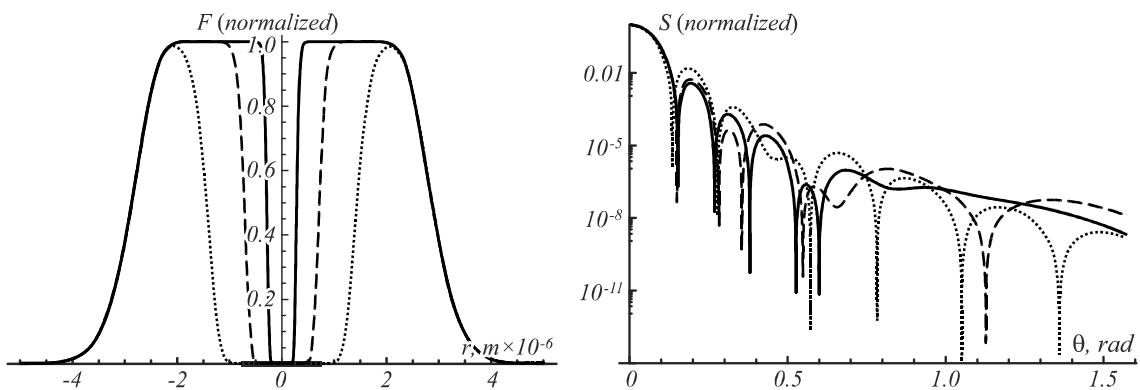


Fig. 3. The potential and the intensity of the scattered plane wave for $L = 40$, $\sigma_o = 10/k$ and different thickness $\sigma_i = 1/k$ (solid curve), $\sigma_i = 2.5/k$ (dashed curve), $\sigma_i = 5/k$ (dotted curve)

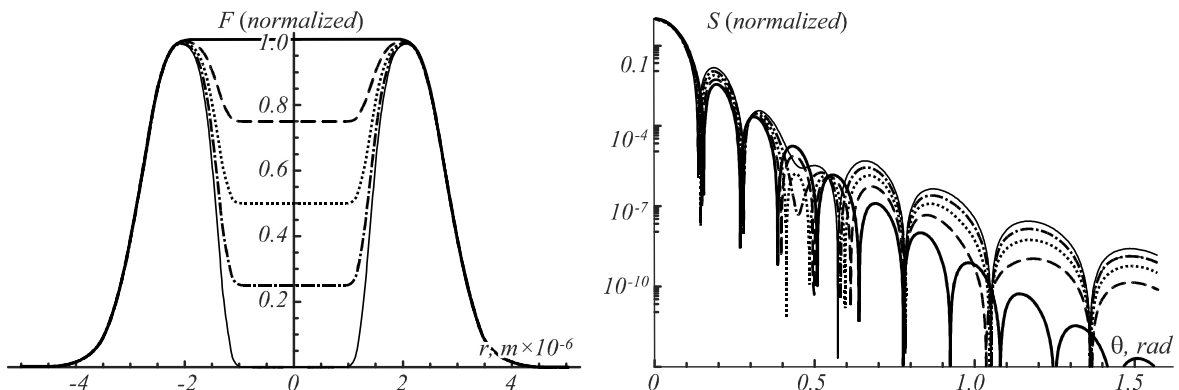


Fig. 4. The semi-hollow potentials and the corresponding intensity of the plane wave scattered from them for $h_i = 0$ (thick solid curve), $h_i = 0.25$ (dashed curve), $h_i = 0.5$ (dotted curve), $h_i = 0.75$ (dash-dotted curve) and $h_i = 1$ (thin solid curve)

Where the similar condition must be satisfied since the minimum value of the potential and the thickness are nonnegative. So $h_o > h_i$, $\sigma_{xo} > \sigma_{xi}$, $\sigma_{yo} > \sigma_{yi}$, $\sigma_{zo} > \sigma_{zi}$.

Figure 5(a) and 5(b) illustrate the hollow ellipsoidal potentials with $L=1$ and $L=20$, respectively. As the upper index increases the ellipsoidal shell with sharper inner and outer edges is formed.

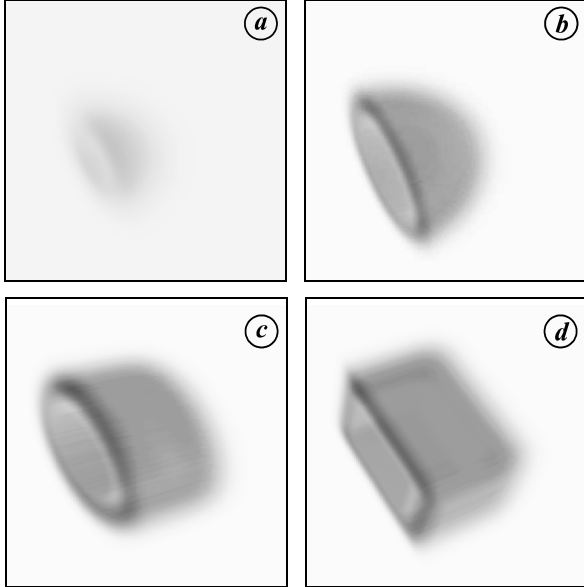


Fig. 5. Hollow (a) ellipsoid with $L=1$, (b) ellipsoid with $L=20$, (c) cylinder with $L=M=20$ and (d) parallelepiped with $L=M=P=20$. For all figures $\sigma_{xo} > 1/k$, $\sigma_{yo} > 1.5/k$, $\sigma_{zo} > 2/k$, $\sigma_{xi} > 0.5/k$, $\sigma_{yi} > 1/k$ and $\sigma_{zi} > 1.5/k$

On substituting this expression into Eq. (3) one finds that the corresponding far field scattered intensity becomes

$$S_{HE}^{(s)}(rs; \omega) = \frac{S^{(i)}(\omega)k^2}{4\pi r^2} \left\{ h_o \frac{(2\pi)^{3/2} \sigma_{xo} \sigma_{yo} \sigma_{zo}}{C_l} \times \sum_{l=1}^L \frac{(-1)^{l-1}}{l^{3/2}} \binom{L}{l} \exp \left[\frac{-k^2}{2l} (\sigma_{xo}^2 (\mathbf{s}_x - \mathbf{s}_{0x})^2 + \sigma_{yo}^2 (\mathbf{s}_y - \mathbf{s}_{0y})^2 + \sigma_{zo}^2 (\mathbf{s}_z - \mathbf{s}_{0z})^2) \right] - h_i \frac{(2\pi)^{3/2} \sigma_{xi} \sigma_{yi} \sigma_{zi}}{C_l} \sum_{l=1}^L \frac{(-1)^{l-1}}{l^{3/2}} \binom{L}{l} \times \exp \left[\frac{-k^2}{2l} (\sigma_{xi}^2 (\mathbf{s}_x - \mathbf{s}_{0x})^2 + \sigma_{yi}^2 (\mathbf{s}_y - \mathbf{s}_{0y})^2 + \sigma_{zi}^2 (\mathbf{s}_z - \mathbf{s}_{0z})^2) \right] \right\}^2 \quad (14)$$

Similarly the following condition must be satisfied.

$$h_o \sigma_{ox} \sigma_{oy} \sigma_{oz} - h_i \sigma_{ix} \sigma_{iy} \sigma_{iz} \geq 0. \quad (15)$$

And this is also automatically satisfied because of the previous condition. Fig. 6 presents the density plots of the plane wave scattered from a typical ellipsoidal potential of fixed size with solid [6(a) and 6(c)] and completely hollow [6(b) and 6(d)] centers. Soft-edge case ($L=1$, [6(a) and 6(b)]) and fairly hard-edge case ($L=40$, [6(c) and 6(d)]) are considered. Compared with soft-edge, the

hard-edge case lead to increased number of dark fringes. And in the soft-edge case, two dark fringes appear in the center in the hollow potentials. In the hard-edge case, compared with solid potentials the hollow potentials lead to reduced number of dark fringes.

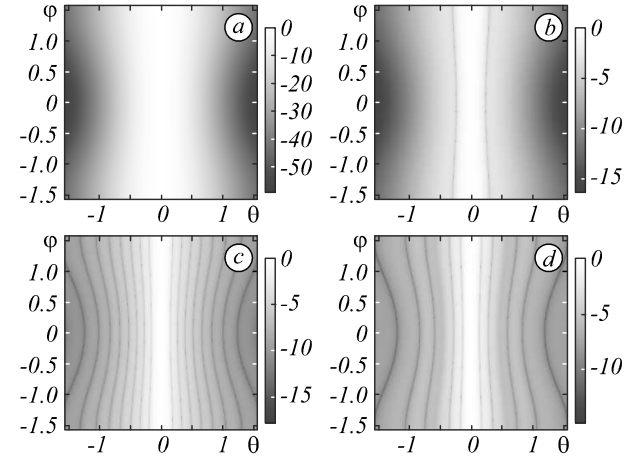


Fig. 6. Density plots of the scattered intensity of a plane wave from ellipsoidal potentials with $\sigma_{ox} = 10/k$, $\sigma_{oy} = 8/k$, $\sigma_{oz} = 6/k$, $\sigma_{ix} = 5/k$, $\sigma_{iy} = 4/k$, $\sigma_{iz} = 3/k$ and (a) $L=1$, $h_i=0$; (b) $L=1$, $h_i=1$; (c) $L=40$, $h_i=0$ and (d) $L=40$, $h_i=1$

4. Hollow Cylinders

The potential of a hollow cylinder-like scatterer with semi-soft edges may be modeled by multiplying a difference of two 1D multi-Gaussian distributions corresponding to the axis of cylinder's symmetry and a difference of two 2D multi-Gaussian distributions corresponding to the other two orthogonal coordinates. For instance a cylinder aligned with the scattered direction z has the potential of the form:

$$F_{HC}(\mathbf{r}; \omega) = \frac{h_0 k^2}{4\pi C_l} \sum_{l=1}^L (-1)^{l-1} \binom{L}{l} \times \exp \left[-l \left(\frac{x^2}{2\sigma_{xo}^2} + \frac{y^2}{2\sigma_{yo}^2} \right) \right] \times \frac{1}{C_m} \sum_{m=1}^M (-1)^{m-1} \binom{M}{m} \exp \left[-m \frac{z^2}{2\sigma_{zo}^2} \right] - \frac{h_i k^2}{4\pi C_l} \sum_{l=1}^L (-1)^{l-1} \binom{L}{l} \exp \left[-l \left(\frac{x^2}{2\sigma_{xi}^2} + \frac{y^2}{2\sigma_{yi}^2} \right) \right] \times \frac{1}{C_m} \sum_{m=1}^M (-1)^{m-1} \binom{M}{m} \exp \left[-m \frac{z^2}{2\sigma_{zi}^2} \right]. \quad (16)$$

Where the similar condition must be satisfied. Here C_m has the same form as C_l in (6) but generally different value of upper index. In order to model a potential aligned with x or y directions it suffices to exchange in (16) all the quantities relating to z direction with those relating to x or y directions.

Figure 5(c) shows the hollow cylindrical potential with $L=M=20$. We note that for $L=M=1$ the cylinder reduces to the Gaussian shell in 5(a).

Figure 7 shows typical distributions of scattered intensity of light scattered from cylinders oriented along the

scattering axis and having various potential strength h_i in the center. Generally for cylinders two sets of curves crossing each other appear. As h_i grows from 0 (solid cylinder) to 1 (hollow cylinder) the number of destructive interference curves decreases.

Figure 8 illustrates the interference pattern for cylinders with the axis of symmetry along the direction

perpendicular to that of the incident light wave. In this case for semi-hollow scatterers closed curves in $\theta - \phi$ plane may appear. In addition, the comparison between Figs. 7 and 8 implies that the orientation of the cylinder plays the crucial part for qualitatively determining of the scattered intensity distribution.

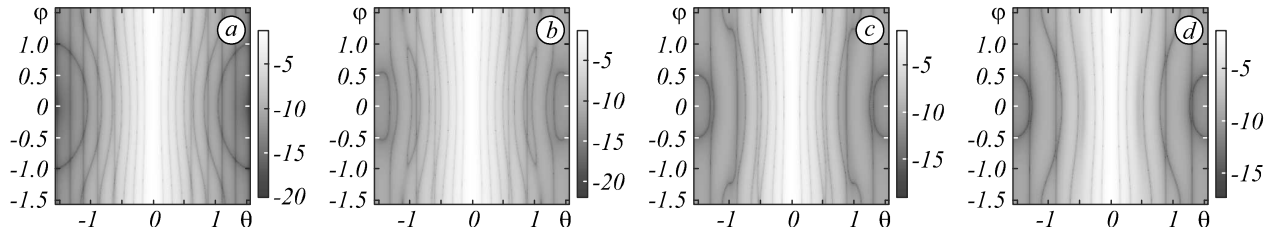


Fig. 7. Density plots of the far-field intensity of the plane wave scattered from the cylindrical scatterers with symmetry axis along the z -direction (coinciding with the scattering axis) with $\sigma_{ox} = 10/k$, $\sigma_{oy} = 8/k$, $\sigma_{oz} = 6/k$, $\sigma_{ix} = 5/k$, $\sigma_{iy} = 4/k$, $\sigma_{iz} = 3/k$ for (a) $h_i = 0$ (solid ellipsoid); (b) $h_i = 0.1$; (c) $h_i = 0.4$; (d) $h_i = 1$ (completely hollow ellipsoid)

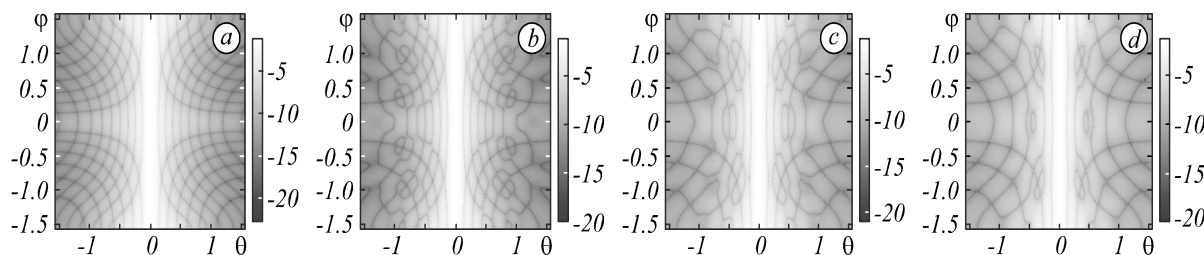


Fig. 8. Density plots of the far-field intensity of the plane wave scattered from the cylindrical scatterers with symmetry axis along the z -direction (perpendicular to the scattering axis) with $\sigma_{ox} = 10/k$, $\sigma_{oy} = 8/k$, $\sigma_{oz} = 6/k$, $\sigma_{ix} = 5/k$, $\sigma_{iy} = 4/k$, $\sigma_{iz} = 3/k$ for (a) $h_i = 0$ (solid cylinder); (b) $h_i = 0.1$; (c) $h_i = 0.4$; (d) $h_i = 1$ (completely hollow cylinder)

On substituting from Eq. (16) into Eq. (3) we find that the corresponding far-field scattered intensity takes the form:

$$\begin{aligned}
 S_{HC}^{(s)}(\mathbf{r}\mathbf{s}; \omega) &= \frac{S^{(i)}(\omega)k^2}{4\pi r^2} \left\{ h_o \frac{(2\pi)^{3/2} \sigma_{xo} \sigma_{yo} \sigma_{zo}}{C_l C_m} \times \sum_{l=1}^L \frac{(-1)^{l-1}}{l} \binom{L}{l} \times \right. \\
 &\times \exp \left[\frac{-k^2}{2l} \left(\sigma_{xo}^2 (\mathbf{s}_x - \mathbf{s}_{0x})^2 + \sigma_{yo}^2 (\mathbf{s}_y - \mathbf{s}_{0y})^2 \right) \right] \times \sum_{m=1}^M \frac{(-1)^{m-1}}{\sqrt{m}} \binom{M}{m} \exp \left[\frac{-k^2 \sigma_{zo}^2}{2m} (\mathbf{s}_z - \mathbf{s}_{0z})^2 \right] - \\
 &- h_i \frac{(2\pi)^{3/2} \sigma_{xi} \sigma_{yi} \sigma_{zi}}{C_l C_m} \sum_{l=1}^L \frac{(-1)^{l-1}}{l} \binom{L}{l} \times \exp \left[\frac{-k^2}{2l} \left(\sigma_{xi}^2 (\mathbf{s}_x - \mathbf{s}_{0x})^2 + \sigma_{yi}^2 (\mathbf{s}_y - \mathbf{s}_{0y})^2 \right) \right] \times \\
 &\left. \times \sum_{m=1}^M \frac{(-1)^{m-1}}{\sqrt{m}} \binom{M}{m} \exp \left[\frac{-k^2 \sigma_{zi}^2}{2m} (\mathbf{s}_z - \mathbf{s}_{0z})^2 \right] \right\}^2.
 \end{aligned} \tag{17}$$

5. Hollow Parallelepipeds

A hollow soft-edge parallelepiped's scattering potential can be modeled by a product of three one-dimensional multi-Gaussian distributions:

$$\begin{aligned}
 F_{HP}(\mathbf{r}; \omega) &= \frac{h_0 k^2}{4\pi C_n} \sum_{n=1}^N (-1)^{n-1} \binom{N}{n} \exp \left[-n \frac{x^2}{2\sigma_{xo}^2} \right] \frac{1}{C_p} \sum_{p=1}^P (-1)^{p-1} \binom{P}{p} \exp \left[-p \frac{y^2}{2\sigma_{yo}^2} \right] \times \\
 &\times \frac{1}{C_m} \sum_{m=1}^M (-1)^{m-1} \binom{M}{m} \exp \left[-m \frac{z^2}{2\sigma_{zo}^2} \right] - \frac{h_i k^2}{4\pi C_n} \sum_{n=1}^N (-1)^{n-1} \binom{N}{n} \exp \left[-n \frac{x^2}{2\sigma_{xi}^2} \right] \times \\
 &\times \frac{1}{C_p} \sum_{p=1}^P (-1)^{p-1} \binom{P}{p} \exp \left[-p \frac{y^2}{2\sigma_{yi}^2} \right] \frac{1}{C_m} \sum_{m=1}^M (-1)^{m-1} \binom{M}{m} \exp \left[-m \frac{z^2}{2\sigma_{zi}^2} \right],
 \end{aligned} \tag{18}$$

where C_n and C_p have the same form as normalization factor C_l in (6) but possibly different values of their upper indexes and also the similar condition should be satisfied.

Figure 5(d) shows the hollow parallelepiped-like potential with $L = M = P = 20$. Just like in the cylindrical case, for $L = M = P = 1$ the parallelepiped shell reduces to the elliptical soft Gaussian shell in 5(a).

The far-zone scattered intensity distribution is now readily obtained on substituting from (18) into (3):

$$\begin{aligned}
 S_{HP}^{(s)}(r\mathbf{s}; \omega) = & \frac{S^{(i)}(\omega)k^2}{4\pi r^2} \left\{ \frac{(2\pi)^{3/2} \sigma_{x_0} \sigma_{y_0} \sigma_{z_0}}{C_n C_p C_m} \sum_{n=1}^N \frac{(-1)^{n-1}}{\sqrt{n}} \binom{N}{n} \exp\left[\frac{-k^2 \sigma_{x_0}^2}{2n} (\mathbf{s}_x - \mathbf{s}_{0x})^2\right] \times \right. \\
 & \times \sum_{p=1}^P \frac{(-1)^{p-1}}{\sqrt{p}} \binom{P}{p} \exp\left[\frac{-k^2 \sigma_{y_0}^2}{2p} (\mathbf{s}_y - \mathbf{s}_{0y})^2\right] \left. \sum_{m=1}^M \frac{(-1)^{m-1}}{\sqrt{m}} \binom{M}{m} \exp\left[\frac{-k^2 \sigma_{z_0}^2}{2m} (\mathbf{s}_z - \mathbf{s}_{0z})^2\right] - \right. \\
 & - \frac{(2\pi)^{3/2} \sigma_{x_i} \sigma_{y_i} \sigma_{z_i}}{C_n C_p C_m} \sum_{n=1}^N \frac{(-1)^{n-1}}{\sqrt{n}} \binom{N}{n} \exp\left[\frac{-k^2 \sigma_{x_i}^2}{2n} (\mathbf{s}_x - \mathbf{s}_{0x})^2\right] \sum_{p=1}^P \frac{(-1)^{p-1}}{\sqrt{p}} \binom{P}{p} \exp\left[\frac{-k^2 \sigma_{y_i}^2}{2p} (\mathbf{s}_y - \mathbf{s}_{0y})^2\right] \times \\
 & \left. \times \sum_{m=1}^M \frac{(-1)^{m-1}}{\sqrt{m}} \binom{M}{m} \exp\left[\frac{-k^2 \sigma_{z_i}^2}{2m} (\mathbf{s}_z - \mathbf{s}_{0z})^2\right] \right\}^2. \tag{19}
 \end{aligned}$$

Figure 9 shows the scattered intensity patterns for several parallelepiped-like particles with different values of h_i . Solid [9(b)], semi-solid [9(b) and 9(c)] and hollow [9(d)] scatterers all have three sets of dark curves. Just like in the case of a cylinder, as h_i grows bigger, the dark closed curves may appear for semi-solid scatterers.

Figure 10 compares the scattered intensity patterns for light scattered from completely hollow parallelepipeds with different thickness: thicker walls of the scatterer [Fig. 10(b)] lead to fewer interference curves but more closed curves in the center.

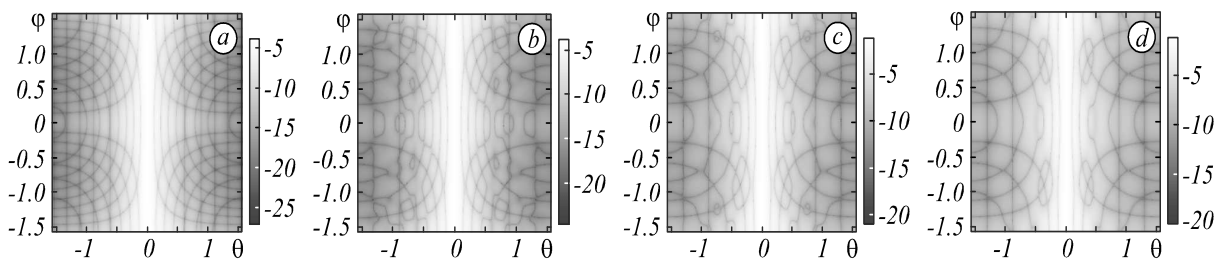


Fig. 9. Density plots of the far-field intensity of the plane wave scattered from the typical parallelepiped-like scatterers with $\sigma_{ox} = 10/k$, $\sigma_{oy} = 8/k$, $\sigma_{oz} = 6/k$, $\sigma_{ix} = 5/k$, $\sigma_{iy} = 4/k$, $\sigma_{iz} = 3/k$ for (a) $h_i = 0$ (solid parallelepiped); (b) $h_i = 0.1$; (c) $h_i = 0.4$; (d) $h_i = 1$ (completely hollow parallelepiped)

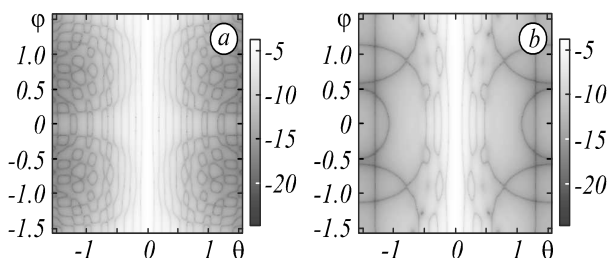


Fig. 10. Density plots of the far-field intensity of the plane wave scattered from two completely hollow parallelepiped-like scatterers ($h_i = 1$) with $\sigma_{ox} = 10/k$, $\sigma_{oy} = 8/k$, $\sigma_{oz} = 6/k$ but of different thickness: (a) $\sigma_{ix} = 9/k$, $\sigma_{iy} = 7/k$, $\sigma_{iz} = 5/k$ and (b) $\sigma_{ix} = 2.5/k$, $\sigma_{iy} = 2/k$, $\sigma_{iz} = 1.5/k$

6. Summary

By means of multi-Gaussian functions in 1D, 2D and 3D settings we have established analytical models for the scattering potentials that can be of different shapes: spherical, ellipsoidal, cylindrical and parallelepiped-like, as well as have adjustable size, outer and inner edge sharpness and shell thickness. On the basis of the first Born approximation and far-zone approximation we have analytically evaluated the distributions of scattered intensities for all the cases for the incident plane wave. Our results illustrate that the solid, semi-hollow and hollow scatterers lead to qualitatively different far-field intensity

distributions, forming the fringe-like patterns accounting for size, sharpness, and geometrical features as the presence of right-angle side-joints (cylinder and parallelepiped) and the corners (parallelepiped). The models are of acute academic interest since they are entirely based on the dimension-separable and easily integrable and transformable Gaussian functions.

The model can be readily extended to the following cases: 1) The choice of different upper indexes for the potentials can account for situations in which different smoothing is required in the three orientations; 2) The profile of the hollow part of the scatterer does not need to coincide with that of the external edge, for instance one can readily model a cube with the removed ellipsoidal central part; 3) The nested potentials of the same or different geometrical profiles can be employed; 4) Multiple exclusions at different locations within the scatterer can be used for modeling of the porous media.

References

- [1] Mie G. Beitrage zur Optik truber Medien, speziell kolloidaler Metallosungen. Annalen der Physik 1908; 330(3): 377-445. DOI: 10.1002/andp.19083300302.
- [2] Wang T, Li X, Ji X, Zhao D. Spectral changes and spectral switches of light waves on scattering from a semisoft boundary medium. Opt Commun 2014; 324: 152-156. DOI: 10.1016/j.optcom.2014.03.054.

- [3] Naraghi RR, Sukhov S, Dogariu A. Directional control of scattering by all-dielectric core-shell spheres. *Opt Lett* 2015; 40(4): 585-588. DOI: 10.1364/OL.40.000585.
- [4] Wang T, Jiang Z, Ji X, Zhao D. Can different media generate scattered field with identical spectral coherence? *Opt Commun* 2016; 363: 134-137. DOI: 10.1016/j.optcom.2015.11.017.
- [5] Wang T, Zhiang Z, Zhu L, Li X. The spectrum of light wave on scattering from an anisotropic semisoft-boundary medium. *Optik* 2016; 127(20): 9231-9235. DOI: 10.1016/j.ijleo.2016.06.116.
- [6] Wang T, Jiang Z, Ji X, Zhao D. Spectrum of an electromagnetic light wave on scattering from an anisotropic semisoft boundary medium. *J Opt Soc Am A* 2016; 33(4): 625-629. DOI: 10.1364/JOSAA.33.000625.
- [7] Li J, Korotkova O. Scattering of light from a stationary nonuniformly correlated medium. *Opt Lett* 2016; 41(11): 2616-2619. DOI: 10.1364/OL.41.002616.
- [8] Zhou J, Zhao D. Scattering of an electromagnetic light wave from a quasi-homogeneous medium with semisoft boundary. *Phys Lett A* 2016; 380(37): 2999-3006. DOI: 10.1016/j.physleta.2016.07.003.
- [9] Zheng G, Ye D, Peng X, Song M, Zhao Q. Tunable scattering intensity with prescribed weak media. *Opt Express* 2016; 24(21): 24169-24178. DOI: 10.1364/OE.24.024169.
- [10] Sharma SK, Somerford DJ. *Light scattering by optically soft particles*. Chichester, UK: Praxis Publishing Ltd; 2006. ISBN: 978-3-540-23910-9. DOI: 10.1007/3-540-37664-X.
- [11] Sahin S, Korotkova O, Gbur G. Scattering of light from particles with semisoft boundaries. *Opt Lett* 2011; 36(20): 3957-3959. DOI: 10.1364/OL.36.003957.
- [12] Sahin S, Korotkova O, Shchepakina E. Potential scattering of light from particles of different shapes with semi-hard edges. *J Opt Soc Am A* 2014; 31(8): 1782-1787. DOI: 10.1364/JOSAA.31.001782.
- [13] Born M, Wolf E. *Principles of Optics*. 7th ed. Cambridge: Cambridge University Press; 1999. ISBN 0-521-642221.

Authors' Information

Xi Chen is currently a PhD student of at the Department of Physics, University of Miami, FL. She has received her BS in Applied Physics from Chongqing University, China in 2014. She is now working in the field of classical theoretical and experimental statistical optics. Email: xxc241@miami.edu.

The information about author **Olga Korotkova** you can find on page 623 of this issue.

Code of State Categories Scientific and Technical Information (in Russian – GRNTI): 29.31.15.

Received October 19, 2016. The final version – October 31, 2016.
